

NASA TM-2001-210253



# **A Wind Tunnel Study on the Mars Pathfinder (MPF) Lander Descent Pressure Sensor**

*J. Francisco Soriano, Rachael V. Coquilla, Gregory R. Wilson, Alvin Seiff, and Tomas Rivell*

National Aeronautics and Space Administration  
John F. Kennedy Space Center, Kennedy Space Center, Florida 32899-0001

---

June 2001

# **A Wind Tunnel Study on the Mars Pathfinder (MPF) Lander Descent Pressure Sensor**

J. Francisco Soriano<sup>1</sup>, Rachael V. Coquilla<sup>2</sup>, Gregory R. Wilson<sup>3</sup>, Alvin Seiff<sup>4</sup>, and Tomas Rivell<sup>5</sup>

<sup>1</sup>**Aerospace Engineer and McNair Scholar. NASA Ames Research Center, Moffett Field, California. Now at John F. Kennedy Space Center, Florida.**

<sup>2</sup>**Graduate Research Associate. Mechanical and Aeronautical Engineering Department, University of California, Davis.**

<sup>3</sup>**Faculty Research Associate, Jet Propulsion Laboratory, Pasadena, California.**

<sup>4</sup>**Senior Research Associate, San Jose State University Foundation, San Jose, California.**

<sup>5</sup>**NASA Ames Research Center, Moffett Field, California.**

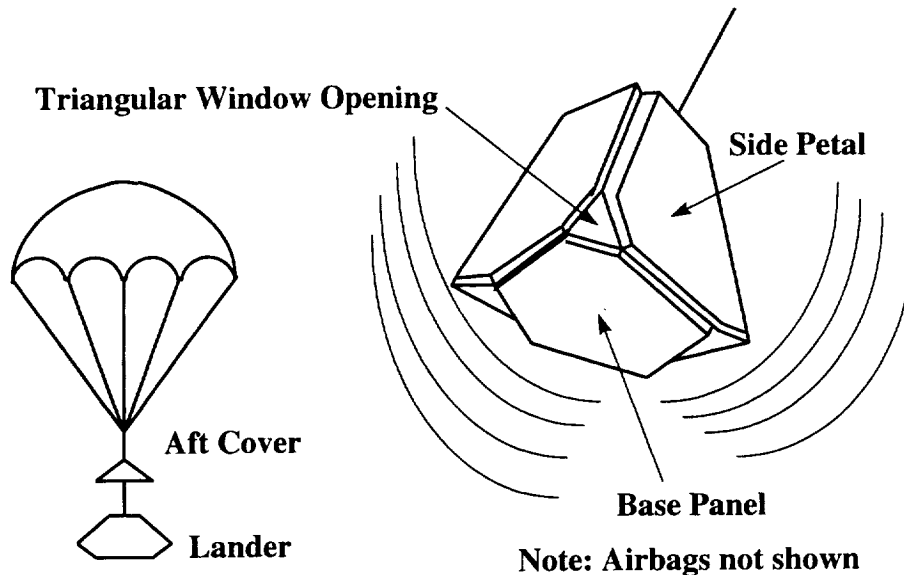
## **ABSTRACT**

The primary focus of this study was to determine the accuracy of the Mars Pathfinder lander local pressure readings in accordance with the actual ambient atmospheric pressures of Mars during parachute descent. In order to obtain good measurements, the plane of the lander pressure sensor opening should ideally be situated so that it is parallel to the freestream. However, due to two unfavorable conditions, the sensor was positioned in locations where correction factors are required. One of these disadvantages is due to the fact that the parachute attachment point rotated the lander's center of gravity forcing the location of the pressure sensor opening to be off tangent to the freestream. The second and most troublesome factor was that the lander descends with slight oscillations that could vary the amplitude of the sensor readings. In order to accurately map the correction factors required at each sensor position, an experiment simulating the lander descent was conducted in the Martian Surface Wind Tunnel at NASA Ames Research Center. Using a 1/5 scale model at Earth ambient pressures, the test settings provided the necessary Reynolds number conditions in which the actual lander was possibly subjected to during the descent. In the analysis and results of this experiment, the readings from the lander sensor were converted to the form of pressure coefficients. With a contour map of pressure coefficients at each lander oscillatory position, this report will provide a guideline to determine the correction factors required for the Mars Pathfinder lander descent pressure sensor readings.

## INTRODUCTION

On July 4, 1997 the Mars Pathfinder lander entered the Martian atmosphere. One component of its science package carried instrumentation aimed to take readings of the ambient pressures during the descent phase. Although measurements were initiated immediately upon entry, the key set of readings that portray the Mars atmosphere were performed immediately after parachute deployment and heat shield ejection until just prior to airbag inflation (see Figure 1).

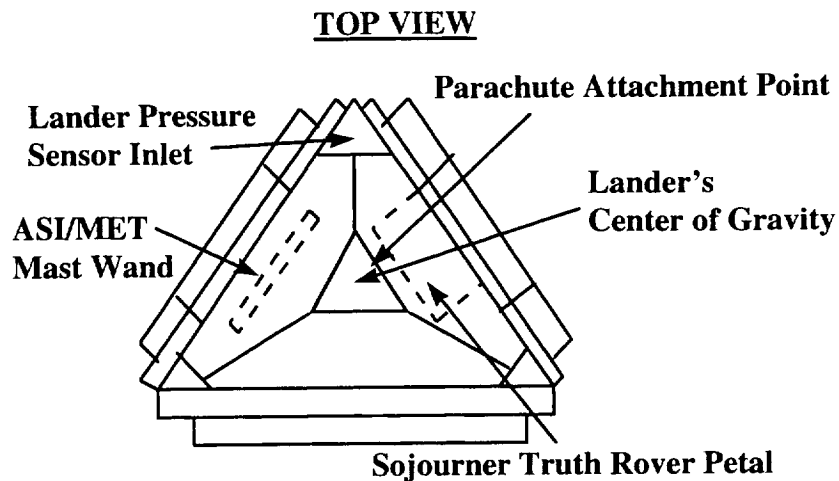
**Figure 1: Mars Pathfinder Lander Parachute Descent Phase**



One of the concerns in the configuration of the spacecraft's atmospheric pressure sensor was to determine how its readings were affected by its position within the lander and with respect to the descent freestream. The sensor is centered and flushed within the triangular window opening formed by the junction of the lander's base and by the two adjacent petals in which one holds the Sojourner Truth rover and the other carries the ASI/MET mast (see Figure 2). Unfortunately, this location of the pressure sensor is also diverted by the rotation of the lander with respect to its parachute. The parachute attachment point is located at the top edge midpoint of the rover petal which forces the center of gravity of the lander to rotate approximately 14 degrees about this attachment point (see Figure 2). Ideally, in order to read ambient pressures, the plane of the

sensor opening should be parallel to the flow. Due to the rotation of the lander, the sensor opening is situated offset from freestream. Additionally, the lander was subjected to varying oscillations during the descent forcing the sensor opening to be positioned in the turbulent wake of the lander side and base platforms or even up to facing against the freestream. Ultimately, with these unfavorable pressure sensor locations, there were times when the readings drew away from the actual atmospheric pressure of Mars.

**Figure 2: Model of the Mars Pathfinder Lander**



In order to find the correction factors at the various sensor positions, a wind tunnel study, simulating the oscillatory Martian descent, was conducted using a 1/5 scale model of the Mars Pathfinder lander. This experiment was performed at the Martian Surface Wind Tunnel which is housed inside a low pressure chamber facility at NASA Ames Research Center, Moffett Field, California. The chamber was originally developed for low pressure acoustic and structural tests on rockets and was later reassigned to accommodate an atmospheric and planetary aeolian wind tunnel. Although the experiment for this study was conducted at Earth atmospheric pressures, it still provided a comparable simulation by duplicating the Reynolds numbers experienced during the descent.

## TEST CONDITIONS

### Conditions to be Simulated

From a previous study which diagrammed the internal and external flow of the Pathfinder lander's Martian descent [Rivell *et al*, 1997], the dynamic conditions inside the wind tunnel were reconstructed for this experiment. According to this investigation, upon parachute deployment and heat shield removal, at approximately 6.0 km above the Martian surface, the lander was predicted to experience a Mach number of 0.48. Based on the full-scale length of one of the side petals' long edges, the Reynolds number is calculated to be  $11.3 \times 10^4$ . During the middle of the descent, variations in velocity and density readings also resulted in acquiring Reynolds numbers ranging from  $12.0 \times 10^4$  to as low as  $8.9 \times 10^4$ .

For the wind tunnel experiment, the freestream velocity was varied to meet the descent Reynolds numbers which were calculated based on the model's side petal edge height.

$$\text{Re} = \frac{\rho_{\infty} V_{\infty} l}{\mu_{\infty}} \quad \text{and} \quad \rho_{\infty} = \frac{P_{\infty}}{R_{\text{AIR}} T_{\infty}}$$

**Re = Measure of the ratio of inertia forces to viscous forces in a flow**

**$V_{\infty}$  = Freestream velocity (m/s)**

**$l$  = Model's side petal edge height (m)**

**$\mu_{\infty}$  = Dynamic viscosity (Ns/m<sup>2</sup>)**

**$P_{\infty}$  = Test section pressure (mb)**

**$R_{\text{AIR}}$  = Universal Gas constant for air (  $8.31441 \times 10^3 \text{ J kmol}^{-1} \text{ K}^{-1}$  )**

**$T_{\infty}$  = Inside chamber temperature (K)**

**$\rho_{\infty}$  = Inside chamber density (kg/m<sup>3</sup>)**

To find the density, both the ambient temperature and pressure were directly measured and were used along with the universal gas constant for air at Earth sea level standard temperature and pressure.

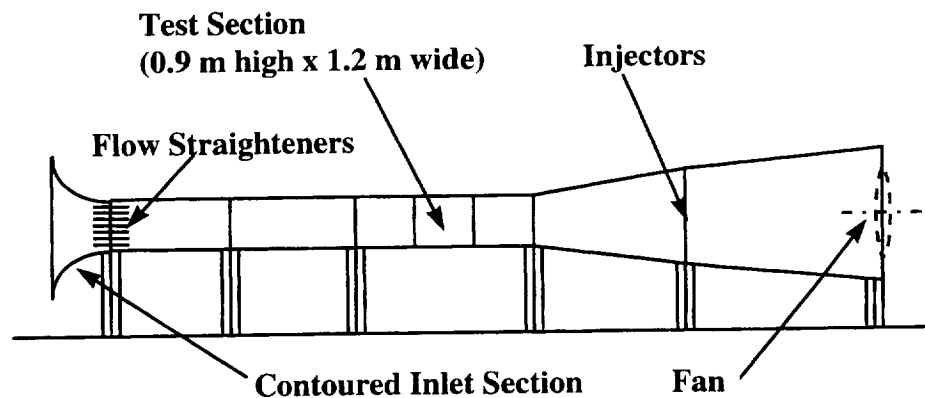
Although the Mach numbers obtained during the experiment were much lower than those of the actual descent ( $< 0.02$ ), duplicating the Mach numbers was, in fact, negligible for the

experiment. Both the descent and experiment Mach numbers were considered to be in the low subsonic speed regime, therefore, compressibility effects were minimal.

### **Martian Surface Wind Tunnel**

Currently managed by Arizona State University, the Martian Surface Wind Tunnel is an open circuit, atmospheric and surface wind tunnel of approximately 13 meters in length with a 1.26 m x 0.96 m test section. It is placed inside a 4,000 m<sup>3</sup> chamber where experiments can be conducted under Earth or Mars atmospheric pressures (see Figure 3). Winds inside the tunnel can be developed in two different methods. When the chamber is maintained at Earth pressures, an electrically powered axial fan at the end of the tunnel is used, creating a maximum velocity of about 12 m/s inside the test section. At low pressure runs, winds are developed by ejecting high velocity air in the rear diffuser section creating a low pressure area downstream of the test section which, in turn, forms a suction through the tunnel. With this method and at a Mars simulated pressure of 4 mb, the tunnel can obtain test section velocities of approximately 100 m/s. In addition, carbon dioxide gas can also be pumped into the chamber to further closely portray the Martian atmosphere.

**Figure 3: Mars Surface Wind Tunnel at NASA Ames Research Center**



In order to obtain several key atmospheric measurements for each experimental run, the wind tunnel is also equipped with various analog instrumentation. Using a Setra model 270 barometer, ambient pressure is measured through a 1.53 mm diameter orifice from the test section ceiling.

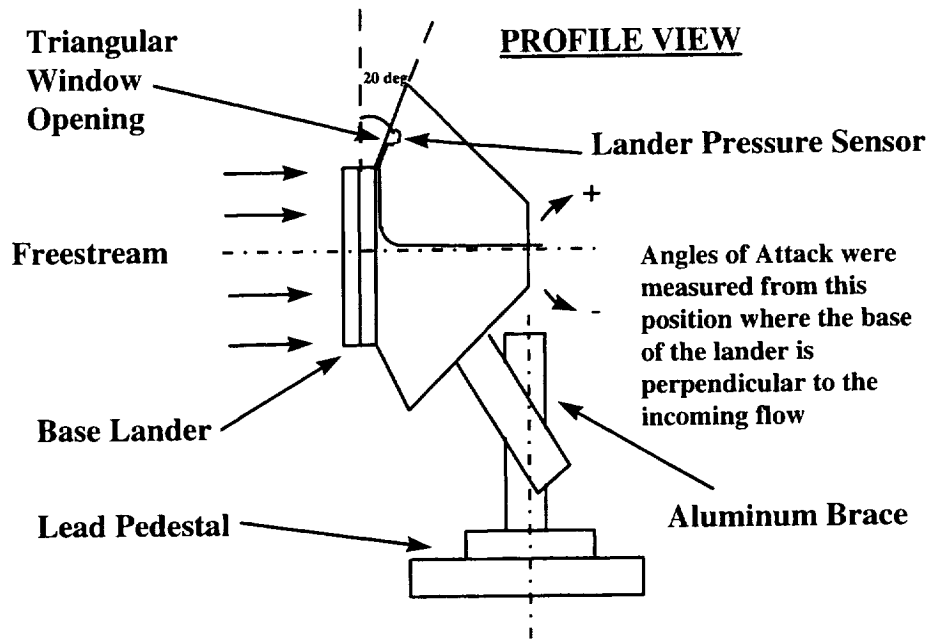
Ambient temperature is measured with a type T thermocouple. For velocity calculations, the test section differential pressure is sensed by a pitot tube equipped with a Setra model 239 differential pressure transducer. Both the thermocouple and the pitot tube are also suspended 13 cm from the test section ceiling, a position in which the ceiling boundary layer and the wake from the lander model do not interfere with their individual readings.

### **Mars Pathfinder Lander Model**

In this experiment a 1/5 scale model of the Mars Pathfinder lander was used. According to previous studies [Rivell *et al.*, 1997], the use of this model inside the Martian Surface Wind Tunnel was verified through potential flow calculations which indicated that the wall turbulence inside the test section would not interfere with the flowfield developed around the model. Based on the scale edge length of one of the side petals and on the maximum test section velocities that can be obtained at both Earth and Mars pressures, this size model can also easily duplicate the Reynolds numbers achieved during the actual Martian descent.

Made of wood, styrene, and transparent acrylic plastic, the model duplicates not only the external size features of the Mars Pathfinder lander but also the approximate size and shape of its major internal structural components, such as the main instrumentation package on the base panel and the Sojourner Truth rover attached to one of the side petals. By recognizing these internal features, the model can also create the general pattern of the lander's internal flow. To secure the model inside the center of the test section, it was mounted to a movable aluminum brace which is connected to the outside center of the side petal that houses no scientific measuring equipment. The brace was then attached onto a heavy lead pedestal with the model's base platform initially facing the incoming flow (see Figure 4).

**Figure 4: Model of the Mars Pathfinder Lander**

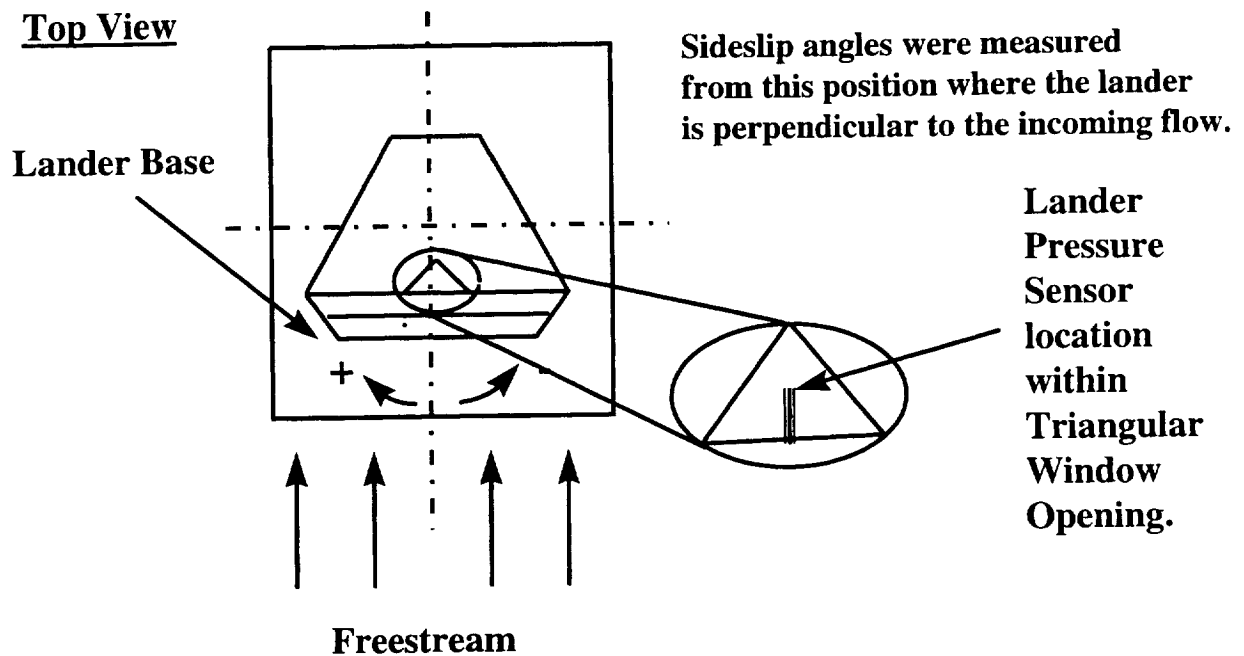


### Experimental Setup

Within the triangular window formed by the rover petal, the ASI/MET mast petal, and the lander base platform, a scaled down version of the atmospheric pressure sensor inlet tube was also added to the model. Based on the spacecraft's design, this particular tube was made only with a single opening in order to attain direct ambient pressure readings. The inlet was connected to a highly sensitive Setra 239 differential pressure transducer. Since this instrument requires readings from two ports, the single-opening lander sensor was connected to the transducer's dynamic port, and a test section ceiling orifice, which is also connected to the barometer, was applied to its reference port. The size of the model dictated a lander sensor opening of 0.2 mm inside diameter. However, with this small opening, the Setra 239 transducer tends to produce uncontrollable pressure fluctuations. Through several tests using various size tubing, starting with the desired scale size, the errors were minimized with a 0.93 mm inside diameter tubing representing a 0.7 scale model. Although this size tubing does not correspond to the scale of the lander model, the distribution of the readings provides the same average as that of the 0.2 scale model. The 0.7 scale tubing simply refines the readings acquired from the smaller tubing.

Therefore, for this experiment a 0.93 mm inside diameter stainless steel tube was conformed to represent the Mars Pathfinder descent pressure sensor (see Figure 5).

**Figure 5: Model of the Mars Pathfinder Lander**



To simulate the Martian descent, the Reynolds numbers for the experiment were varied from  $5.0 \times 10^4$  to  $13.0 \times 10^4$  at increments of  $1.0 \times 10^4$ . With this resolution, a satisfactory set of test runs were conducted at nine different Reynolds numbers. The oscillatory positions were also duplicated by first defining the zero angle from the model and then by applying single longitudinal and lateral rotations. Hence, the reference position was established to be where the lander base platform is perpendicular to the freestream. From this position the top edge of the lander base also defines one side of the triangular window where the lander pressure sensor is situated (see Figure 4). According to the model, the plane of this triangular window was found to be rotated  $20^\circ$  from the lander base platform. By defining the reference position with respect to the base platform and by knowing the location of the sensor window from the base, the position of the lander pressure sensor opening can be determined.

From the zero reference position, a longitudinal rotation or angle of attack was measured using a metal square and protractor against the base platform. Positive angles of attack were designated when the platform is rotated upward. To preset a lateral rotation or sideslip angle, a sheet of paper, precisely drafted with the desired angular positions from the freestream direction, was centered and secured onto the test section floor. The lander model, attached to its stand, was then centered on top of this sheet. Its lead pedestal was then marked depicting the position when the lander base platform is perpendicular to the incoming flow. By positioning the pedestal's marks on a desired angular position defined on the sheet, the lateral rotation of the model's base with respect to the freestream can be determined. The positive sideslip angles were also assigned when the base platform is rotated clockwise and away from the incoming flow.

In deciding the range of angles of attack and sideslip angles to be tested, two factors were considered. One pertained to the rotation of the lander's center of gravity due to the position of the parachute attachment point. The other accounted for the possible lander descent oscillations. As previously stated, since the parachute attachment point is slightly offset from the lander's center of gravity, the lander was assumed to rest at approximately  $14^\circ$  about the attachment point. From the model's zero reference position, this rotation is characterized as  $+7^\circ$  angle of attack and  $+12^\circ$  sideslip (see Figure 2). Based on the predicted descent velocity and atmospheric conditions, the lander was also presumed to oscillate at an amplitude of  $\pm 20^\circ$  from its equilibrium position. Therefore, as shown in Table 1, the sensor positions to be tested were preset using the selected rotation angles measured in degrees.

### **Data Acquisition**

To cover all possible positions in which the lander sensor could oscillate into, the model was first set at a particular angle of attack and then rotated laterally at every sideslip angle. For each angle of attack and sideslip angle position, nine Reynolds number runs were performed. To acquire the readings from all the instruments simultaneously, the Martian Surface Wind Tunnel is outfitted with an automated data acquisition system called LabVIEW, which is also equipped with a local signal conditioning device. Operated through a 100 MHz Pentium processor using Windows '95 and 32.0 MB of RAM, is capable of acquiring voltage readings at rates of up to 1000 Hz, averaging 500 samples per data point. LabVIEW also has the capability to conduct

several simultaneous calculations for each set of data points. Therefore, the acquisition rates primarily depend on the amount of calculations the program performs. Although LabVIEW is capable of carrying out higher sampling rates, the data acquisition was set to 500 Hz, averaging 100 samples per data point over a period of 30 seconds. The lower sample rates were decided primarily due to the amount of calculations that LabVIEW performed.

For this experiment, the program determined the wind tunnel temperature in degree Celsius; the wind tunnel barometric pressure, freestream differential pressure, and lander sensor differential pressure in millibars; the freestream velocity in meters per second; the atmospheric density in kilograms per cubic meter; and the Reynolds number. Despite the lower acquisition rate, LabVIEW was still able to provide a set of 300 data points (means) for each 30 second run.

## RESULTS

With LabVIEW's signal conditioning device, the wind tunnel instruments were maintained with the variations shown in Table 2 and Figures 4-5. Due to wind tunnel vibrations made by the axial fan and to other minor disturbances, the tolerances for the differential pressure readings varied from a minimum of  $\pm 0.009$  mb to the maximum values stated in Table 2. Although the readings from the freestream pitot tube became more erratic with increasing velocity, the test section speeds were still maintained within a maximum variation of  $\pm 0.05$  m/s. Since the lander model pressure sensor was equipped with the more precise and stable transducer, its readings only amplified to a maximum of  $\pm 0.062$  mb.

Although the Reynolds numbers were easily duplicated, the dynamic pressures from the actual descent were of a greater magnitude than those depicted during the wind tunnel experiment. Therefore, in order for the pressure measurements from the lander sensor to be more applicable to any conditions in the low subsonic regime, they were converted in the form of coefficients of pressure,  $C_p$ .

$$C_p = \frac{\Delta p}{q_\infty}$$

$$\Delta p = P_L - P_\infty = \text{Differential pressure (mb)}$$

$$q_\infty = \left(\frac{1}{2}\right) \rho_\infty V_\infty^2 = \text{Dynamic pressure (mb)}$$

$$P_L = \text{Lander pressure (mb)}$$

$$P_\infty = \text{Ambient pressure (mb)}$$

A coefficient of pressure is a dimensionless, similarity parameter used to describe the local surface conditions as a function of the freestream dynamic conditions. Consequently, due to its location within the lander, the pressure sensor inlet was actually sampling local "surface" pressure rather than ambient pressure. Therefore, with the differential pressure ( $\Delta p$ ) readings from the sensor and the dynamic pressure ( $q_\infty$ ) calculations from the test section atmospheric instruments, the sensor pressure coefficient can be determined for each designated lander rotation from the freestream. As long as the Mach number for this approximately blunt-shaped spacecraft

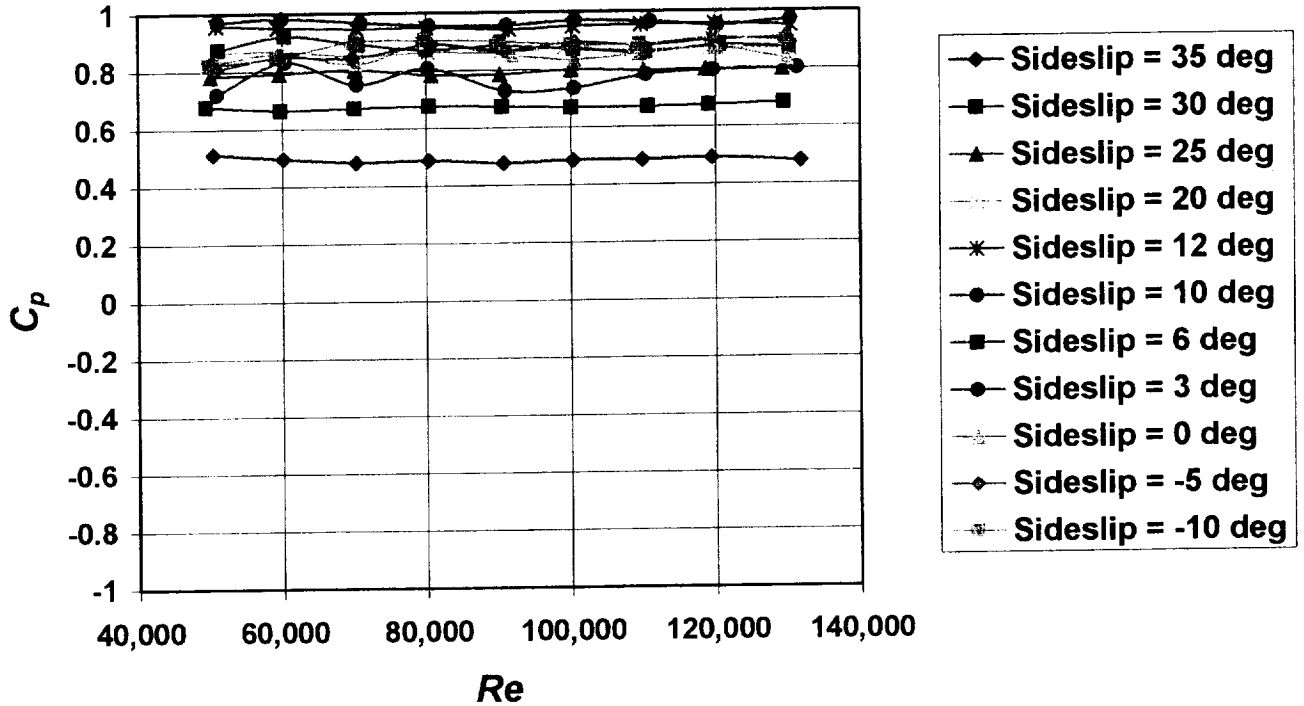
does not exceed a range where compressibility factors are magnified ( $M_\infty \sim 0.8$ ), the pressure coefficients predicted around the model can be referenced to describe the conditions around the actual lander during its descent.

In this report the experimental results are presented in two ways. The first set shows the effect of model rotations against a range of test section Reynolds numbers (Figures 6-15.) To simplify the plots, angle of attack was designated as  $\alpha$  and sideslip angle as  $\beta$ . The next set of results (Figures 16-24) displays the predicted contour maps of  $C_p$  for each Reynolds number tested at various lander rotations from its equilibrium position. Finally, Figures 25-27, display plots of average differential pressure readings, average standard deviations, and average velocity as functions of Reynolds numbers to confirm the legitimacy and accuracy of the data for each experimental run.

### ANALYSIS

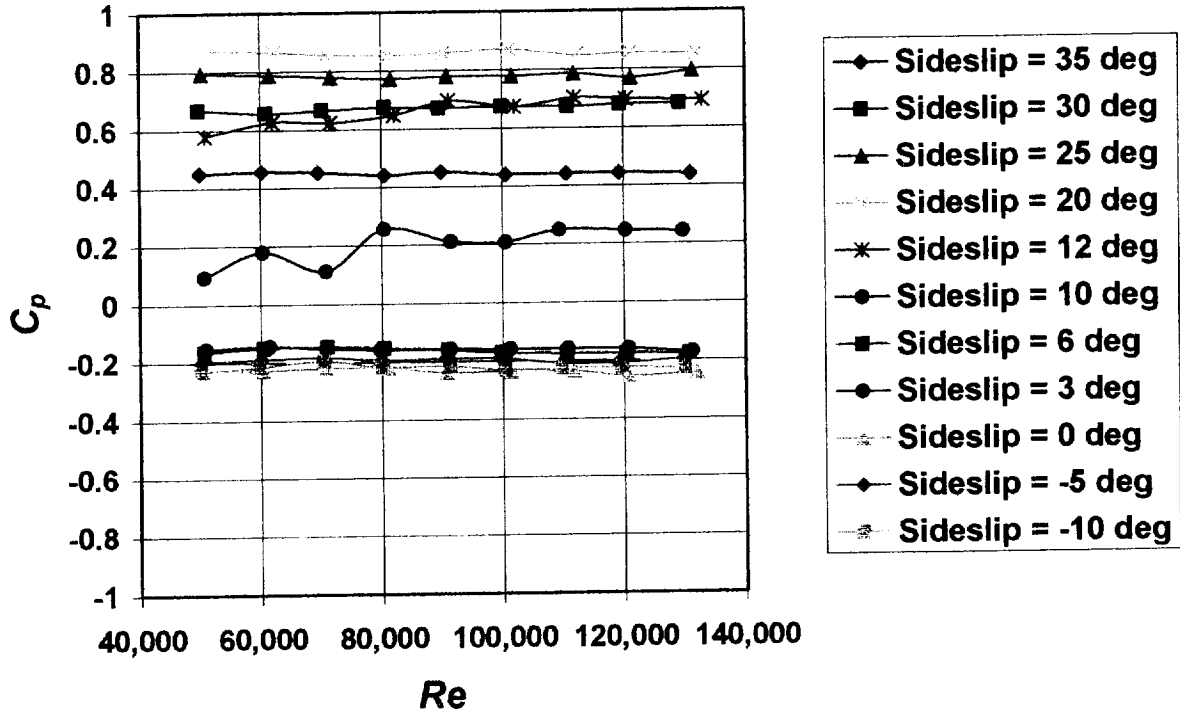
As previously stated in the experimental setup, the lander pressure sensor opening was located at an additional  $20^\circ$  away from the freestream for each angle of attack that the model is rotated. This sensor position is designated in the graphs as  $\alpha_2$ . Through preliminary observations of Figures 6 through 15, the plots revealed concentrations of pressure coefficients approaching one at an initial  $\alpha$  of  $-6^\circ$ , placing the sensor opening at an  $\alpha_2$  of  $14^\circ$  (See Figure 13). As the angle of attack was decreased, the distributions became more uniform with Reynolds number at a particular  $C_p$  for each sideslip position, but yet still closer to one. In particular, these longitudinal rotations completely exposed the lander sensor opening to the incoming flow. As the sensor opening became more perpendicular to the flow, its  $C_p$  values became closer to the value of one which implied that a stagnation point develops at the tip of the sensor.

**Figure 13:  $C_p$  vs  $Re$  for  $\alpha = -6$  deg ( $\alpha_2 = 14$  deg)**



Over the same observations, clusters of negative  $C_p$  were also found to develop at an early  $\alpha$  of  $0^\circ$  in the lower  $\beta$  angles (see Figure 12). In these positions the plane of the sensor opening was still faced against the incoming flow, therefore, the pressure coefficients should have stayed positive. By contrast, positive pressures were not attained until  $\beta$  was increased beyond  $+6^\circ$ . Looking at the approach of the freestream towards the triangular opening which houses the sensor, these premature negative pressure readings were actually caused by the wake from the lander base platform. As  $\beta$  increased, the edge of the platform was also rotated away from the freestream which, in turn, reduced the size of the resulting wake and eventually recovered the presumed positive  $C_p$ .

**Figure 12:  $C_p$  vs  $Re$  for  $\alpha = 0$  deg ( $\alpha_2 = 20$  deg)**

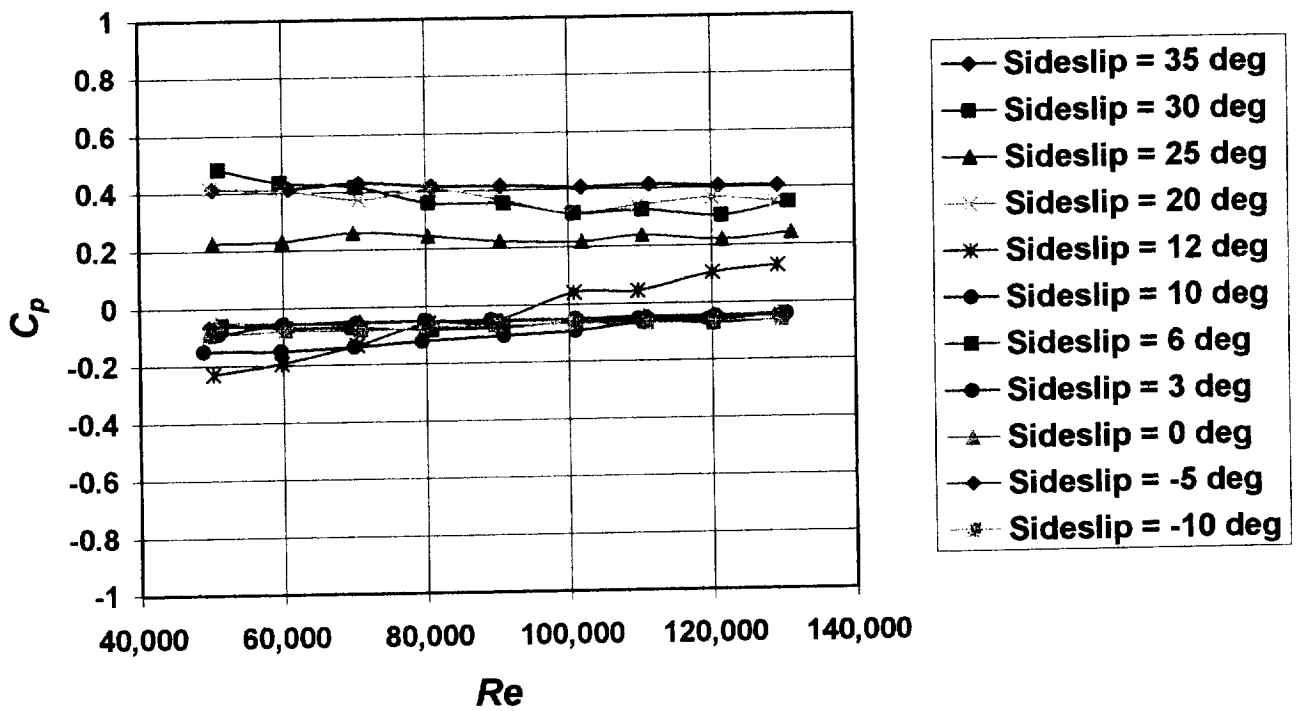


Results (Figure 12) also introduced a variation in pressures at sideslip angles of  $\pm 10^\circ$ . According to the externally symmetrical shape of the model, as it is attached on its stand, these particular lateral rotations should have reported the same pressure readings. Instead, the readings fell within an average pressure coefficient difference of 0.4, where the higher pressure was attained at  $\beta = +10^\circ$ . This difference was possibly due to the presence of the rover structure on one of the side petals. As the freestream reached and entered the window opening, the rover model constricted the flow allowing most of it to escape into one side of the triangular window. As the sideslip was increased from zero, the rover structure forced the entry velocity to increase, thereby allowing the wake from the lander to decrease faster. When  $\beta$  was decreased, the rover structure was not obstructing the entry, hence, the flow only slowly entered the window maintaining a constant size wake and allowing the pressure sensor to acquire negative  $C_p$ .

By increasing the angle of attack, the pressure coefficients for each sideslip angle slowly turned negative. At an  $\alpha$  of  $20^\circ$  (Figure 7), the  $C_p$  distribution began to stabilize at only negative values

which were also distinct for each sideslip angle. Until then, the pressures varied from positive to negative with sideslip angle and, in some cases, with Reynolds number. The variations with  $Re$  were possibly due to the amount of flow entering the triangular window opening. At slower velocity, most of the flow was tripped by the edge of the base platform producing a larger wake over the window and negative pressures from the sensor. As velocity increased, the larger pressure difference between outside and inside the lander created a greater suction through the window opening. This suction decreased the size of the base platform's wake and also began to increase the pressure sensor reading. In Figure 10, this phenomena was greatly revealed at an  $\alpha$  of  $7^\circ$  and  $\beta$  of  $12^\circ$  where the sensor read from negative to positive pressures.

**Figure 10:  $C_p$  vs  $Re$  for  $\alpha = 7$  deg ( $\alpha_2 = 27$  deg)**



Through further evaluations  $C_p$  also showed to be Reynolds number independent with most of the tested lander oscillatory positions. However, there were certain situations where the  $C_p$  drastically changed with Reynolds number. Unfortunately, the most significant occurrence can be seen at the nominal or equilibrium position of  $\alpha = 7^\circ$  and  $\beta = 12^\circ$ , where the  $C_p$  increased from

**Figure 6:  $C_p$  vs Re for  $\alpha = 27$  deg ( $\alpha_2 = 47$  deg)**

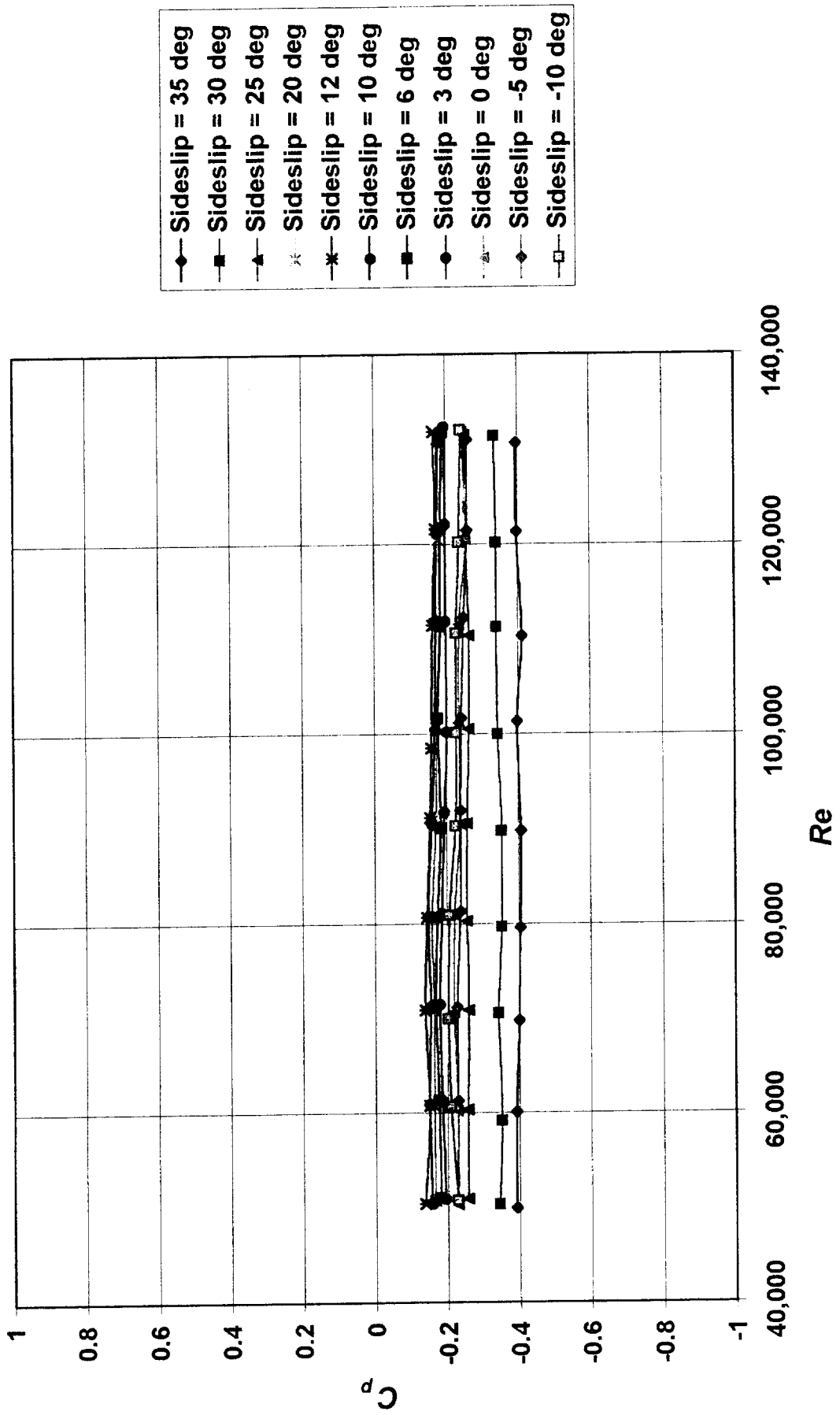


Figure 15:  $C_p$  vs Re for  $\alpha = -16$  deg ( $\alpha_2 = 4$  deg)

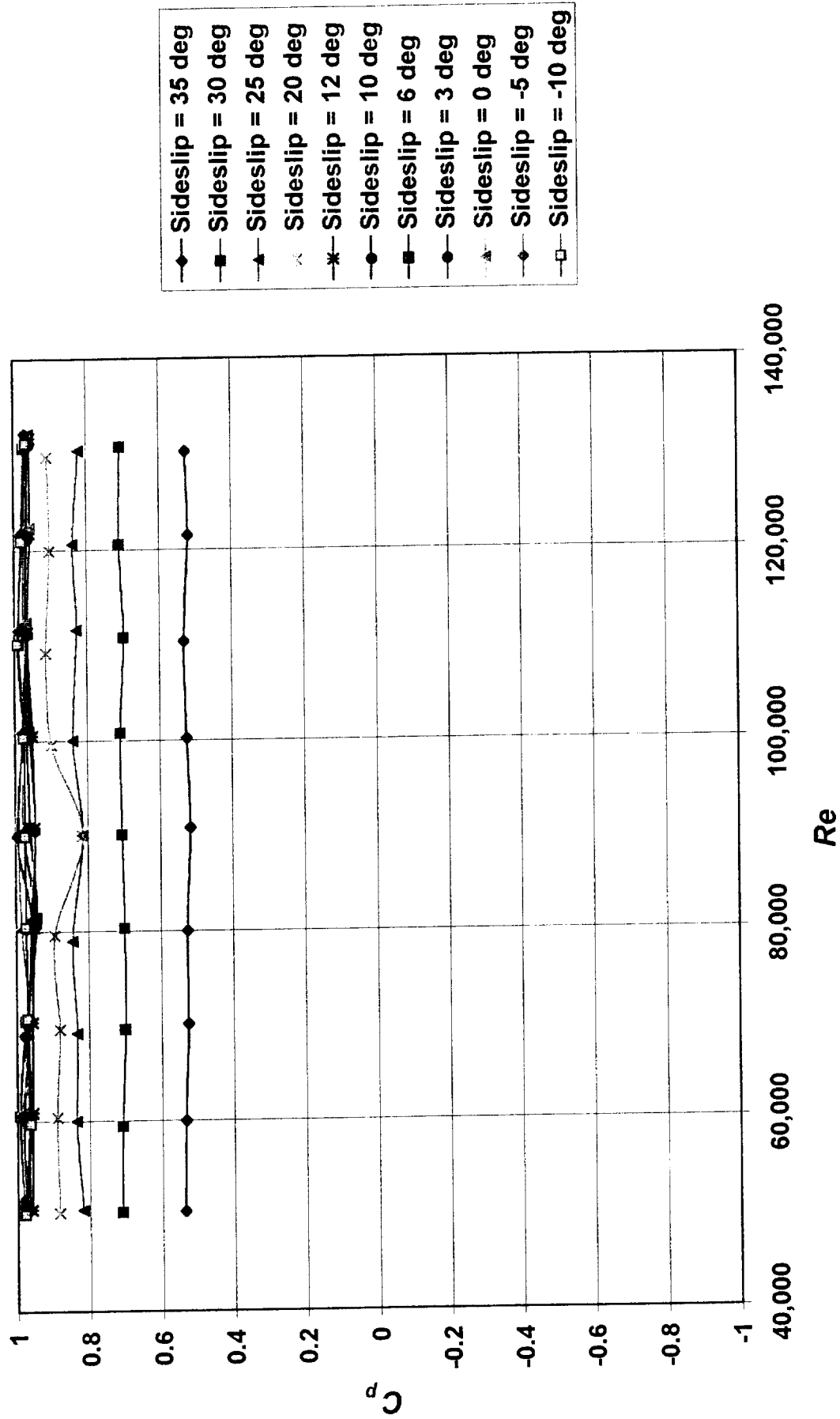
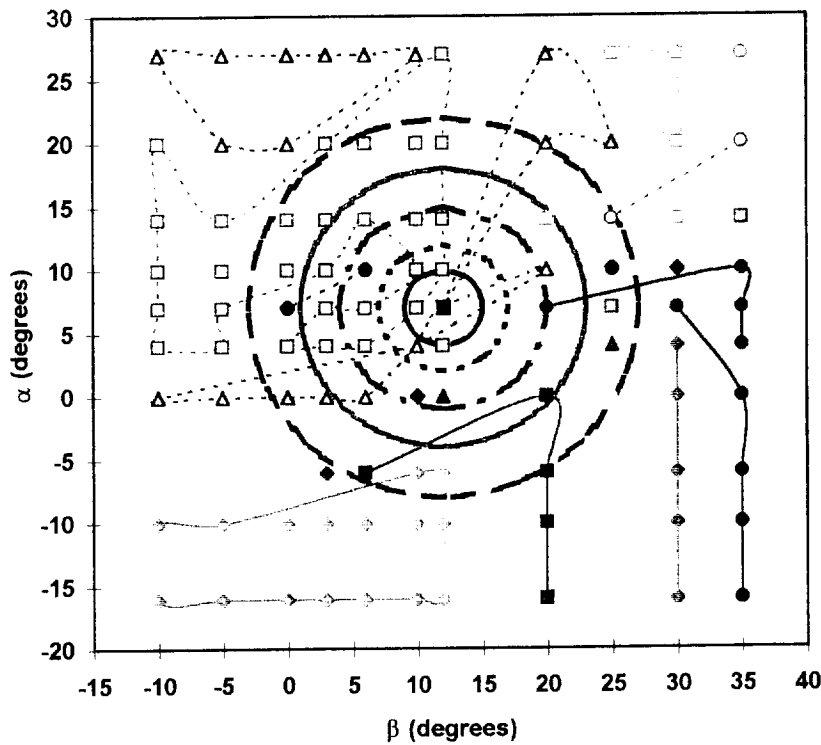
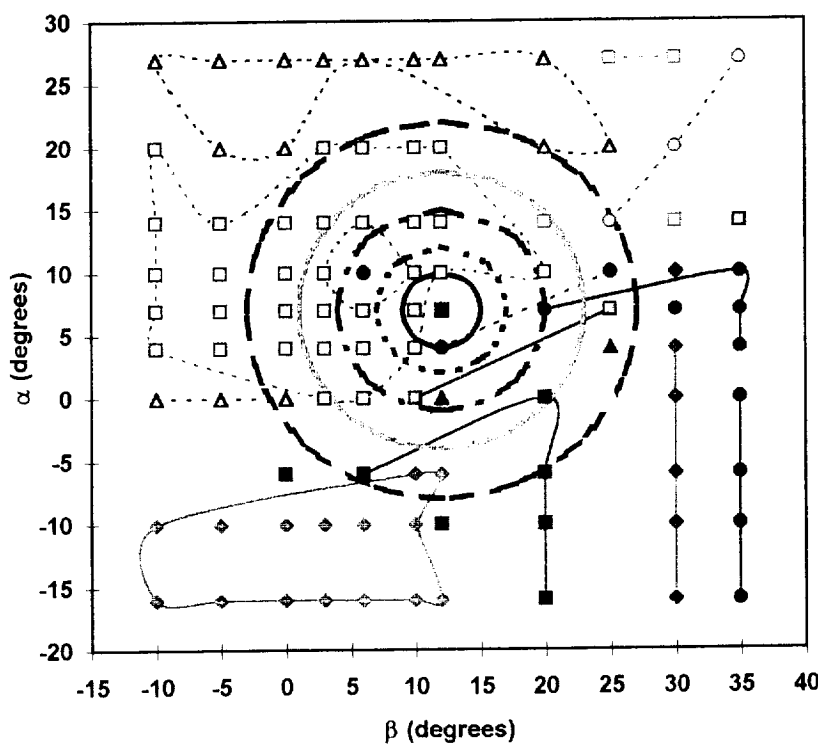


Figure 16: Contours of  $C_p$  for  $Re = 50,000$



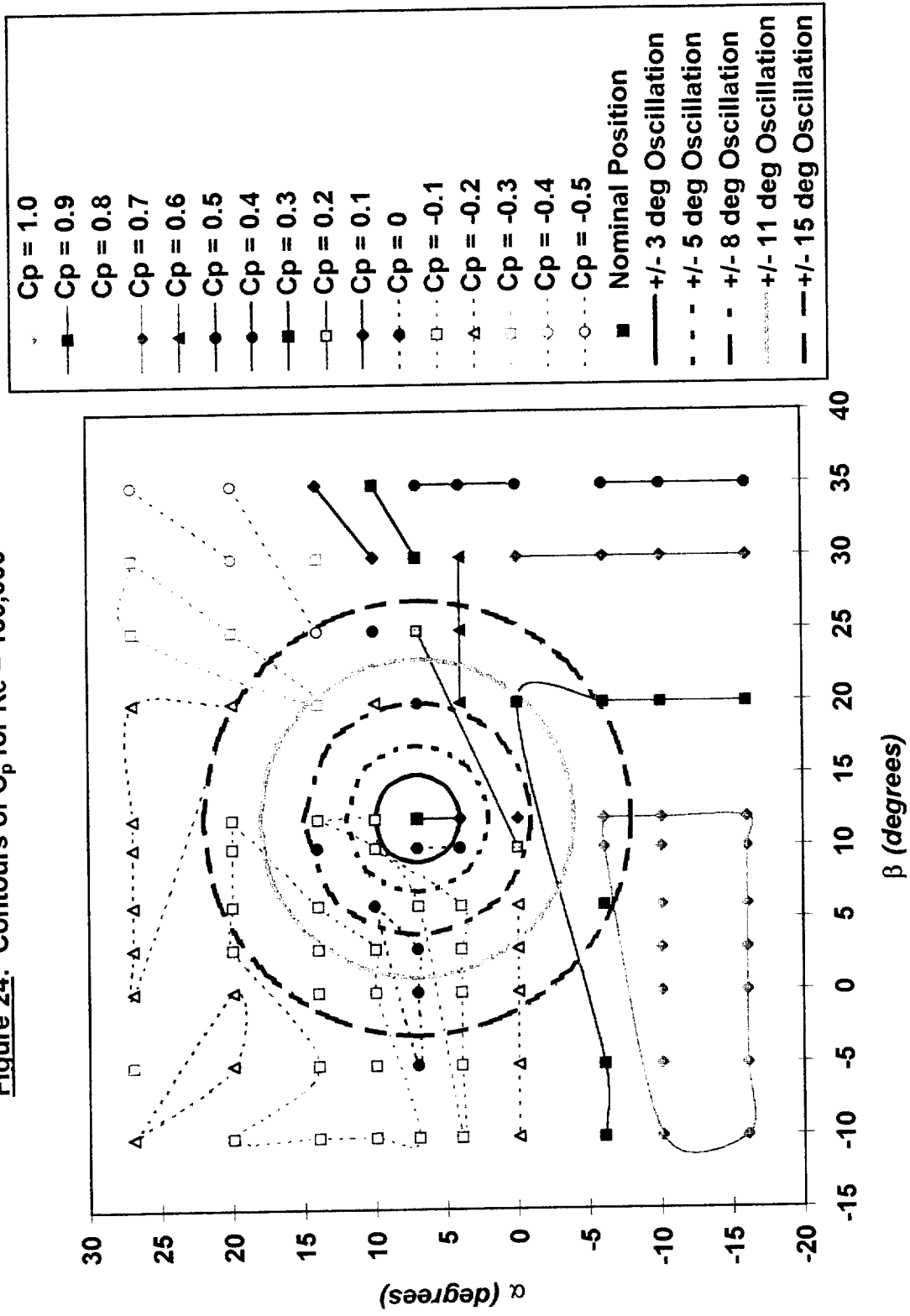
- $C_p = 1.0$
- $C_p = 0.9$
- $C_p = 0.8$
- ◇  $C_p = 0.7$
- ▲  $C_p = 0.6$
- $C_p = 0.5$
- $C_p = 0.4$
- $C_p = 0.2$
- ◆  $C_p = 0.1$
- $C_p = 0$
- $C_p = -0.1$
- △  $C_p = -0.2$
- $C_p = -0.3$
- $C_p = -0.4$
- $C_p = -0.5$
- Nominal Position
- $\pm 3$  deg Oscillation
- - -  $\pm 5$  deg Oscillation
- - -  $\pm 8$  deg Oscillation
- - -  $\pm 11$  deg Oscillation
- - -  $\pm 15$  deg Oscillation

Figure 17: Contours of  $C_p$  for  $Re = 60,000$



- ◇  $C_p = 1.0$
- $C_p = 0.9$
- $C_p = 0.8$
- ◆  $C_p = 0.7$
- ▲  $C_p = 0.6$
- $C_p = 0.5$
- $C_p = 0.4$
- $C_p = 0.2$
- ◆  $C_p = 0.1$
- $C_p = 0$
- $C_p = -0.1$
- △  $C_p = -0.2$
- $C_p = -0.3$
- $C_p = -0.4$
- $C_p = -0.6$
- Nominal Position
- $\pm 3$  deg Oscillation
- - -  $\pm 5$  deg Oscillation
- - -  $\pm 8$  deg Oscillation
- - -  $\pm 11$  deg Oscillation
- - -  $\pm 15$  deg Oscillation

Figure 24: Contours of  $C_p$  for  $Re = 130,000$



**Figure 25: Average Differential Pressure Readings vs Reynolds Number**

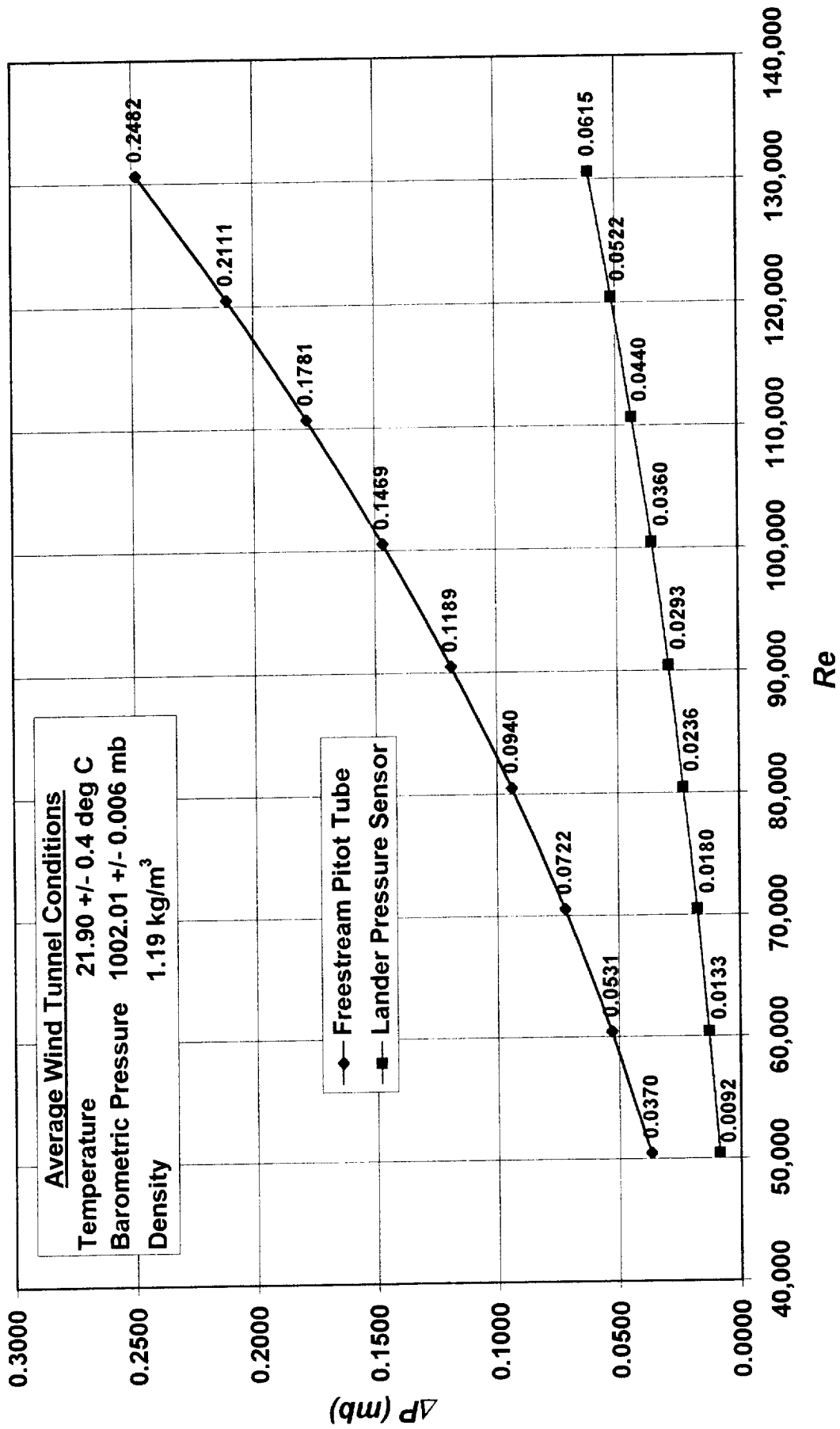


**Figure 26: Average Standard Deviations vs Reynolds Number**

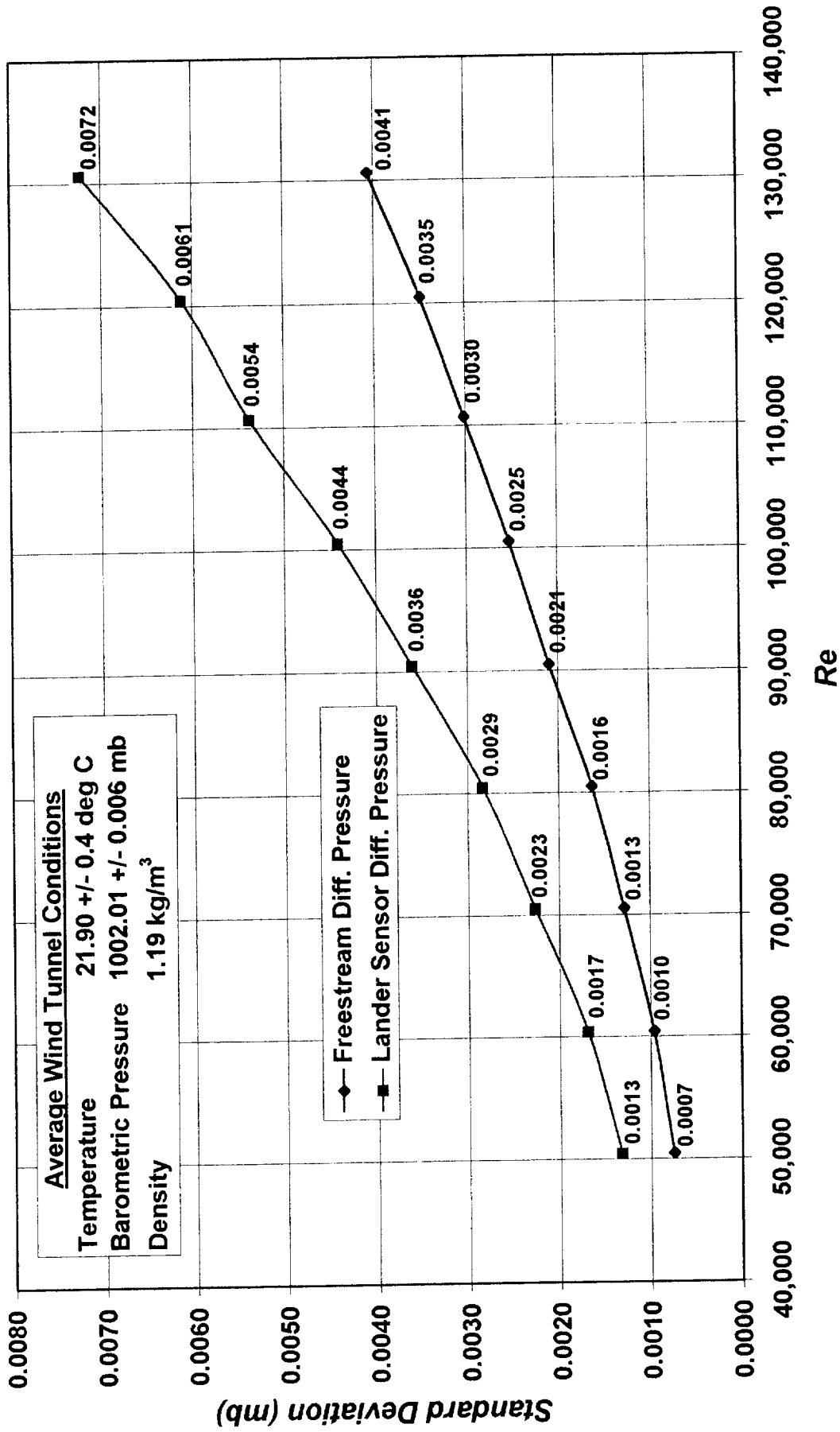
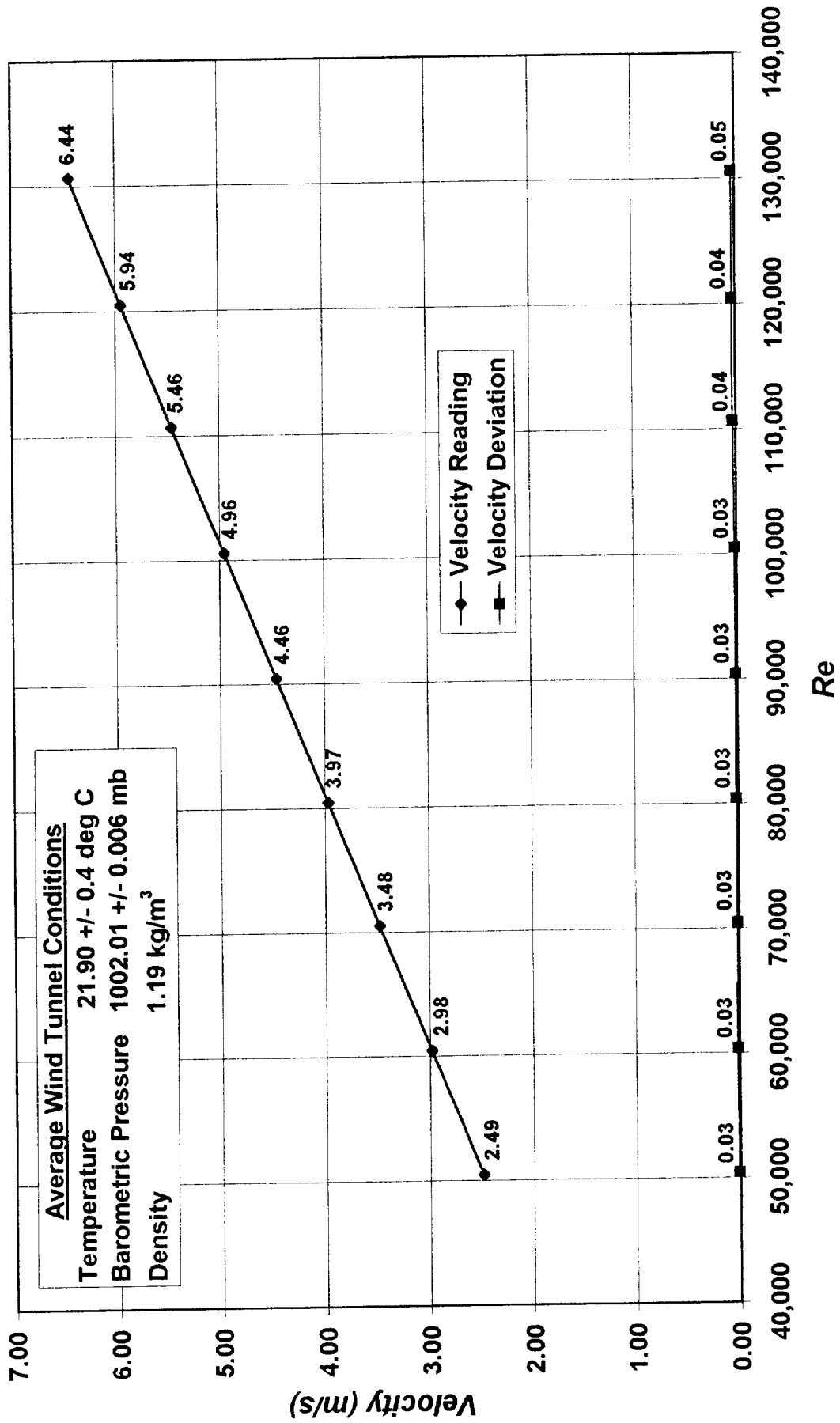


**Figure 27: Average Velocity vs Reynolds Number**



approximately  $-0.22$  at  $Re = 5.0 \times 10^4$  to about  $0.12$  at  $Re = 13.0 \times 10^4$ . In order to account for these inconsistencies,  $C_p$  contour plots were drafted for each Reynolds number experimental run. These contour plots not only display the slight Reynolds number dependency but also predict the  $C_p$  that may generate in a particular region of oscillation.

In Figures 16 through 24 the possible lander oscillations are represented by five concentric circles around the nominal position, while approximate areas of constant  $C_p$  are shown using the various contour lines. Through a general examination, areas of negative pressure were found to be in regions of high  $\alpha$  which are depicted by dotted contour lines, and areas of positive pressure were located in regions of lower  $\alpha$ , identified by solid contour lines. These plots provide a better illustration of the physical interpretation for the Mars Pathfinder lander parachute descent since one can extract from these contour plots, a reasonable range of  $C_p$  that the lander sensor observes at particular spacecraft attitudes. Although there are locations of insufficient data points, such as at  $\beta = 15^\circ$ , these values can be interpolated from the surrounding calculated  $C_p$  values to further improve the resolution.

## APPLICATIONS

At moderate oscillations of about  $\pm 3^\circ$  to  $\pm 8^\circ$ , the pressure sensor is more likely to be measuring a range of  $C_p$  closer to zero, indicating a small pressure correction. However, when the oscillations exceeded these amplitudes, major corrections may be required since at a certain region of oscillation  $C_p$  reaches a value closer to one. By previous definition when  $C_p$  is zero, the lander sensor reading is equal to the ambient pressure (i.e.  $\Delta p = P_L - P_\infty = 0$ ), therefore, no correction is required. For sensor positions where  $C_p$  is steered away from zero, measurements from the Mars Pathfinder's science instruments and the values of  $C_p$  can be used to correct the discrepancies in the descent pressure readings. During its descent Mars Pathfinder employed six sensitive servo accelerometers not only to directly measure spacecraft deceleration, velocity, attitude, and altitude but also to derive the atmospheric density at certain altitudes. Atmospheric temperature was also directly measured using specially designed sensors depicting the same concept as hot wire anemometers [Seiff *et al.*, 1997]. With the temperature and density readings and the ideal gas law, a preliminary ambient pressure can be calculated. By also knowing the

attitude of the spacecraft, the predicted  $C_p$  value from the pressure sensor can be determined and corresponded in the contour plots provided in the results section.

With the readings from the science instruments and the predicted value of  $C_p$ , a correction factor can be determined by means of the following example. Assuming a sample Martian descent condition of  $M_\infty = 0.4$  and  $\gamma = 1.28$  and a preliminary ambient pressure of  $P_\infty = 4$  mb, the dynamic pressure ( $q_\infty$ ) is calculated to be 0.41 mb. By applying an extreme of  $C_p = -2.5$ ,  $\Delta p$  becomes -0.256 mb which corresponds to a 25.6% pressure difference between the lander sensor surface pressure reading and the preliminary ambient pressure. Therefore, using the  $C_p$  values from the experiment and the spacecraft's accelerometer data, the discrepancies in the pressure sensor can be corrected.

**Table 1: Mars Pathfinder Lander Model Rotation Angles**

Angle of Attack	Sideslip Angle
-16	-10
-10	-5
-6	0
0	+3
+4	+6
+7	+10
+10	+12
+14	+20
+20	+25
+27	+30
	+35

**Table 2: Wind Tunnel Instrument Accuracy**

Instrument	Measured Parameter	Accuracy
Type T Thermocouple	Ambient Temperature	$\pm 0.4$ °C
Setra Model 270 Barometer	Ambient Pressure	$\pm 0.006$ mb
Setra Model 239 Transducer	Freestream Differential Pressure	maximum $\pm 0.005$ mb
Setra Model 239 Transducer	Lander Sensor Differential Pressure	maximum $\pm 0.008$ mb

## REFERENCES

<sup>1</sup>Seiff, A., Tillman, J. E., Murphy, J. R., Schofield, J. T., Crisp, D., Barnes, J. R., LaBaw, C., Mahoney, C., Mihalov, J. D., Wilson, G. R., and Haberle, R., "The Atmosphere structure and meteorology instrument of the Mars Pathfinder lander," *Journal of Geophysical Research (Planets)*, Vol. 102, No. E2, 1997, pp. 4045-4056.

<sup>2</sup>Rivell, T., Seiff, A., Jovic, S., Wilson, G. R., Maa, S., and Castellano, T. P., "Wind-Tunnel Test of Flow Through Mars Pathfinder Lander," *Journal of Spacecraft and Rockets*, Vol. 34, No. 3, 1997, pp. 265-271.

<sup>3</sup>White, B. R., "AIAA-87-0291 A Low-Density Boundary-Layer Wind Tunnel Facility," *AIAA 25<sup>th</sup> Aerospace Sciences Meeting*, January 12-15, 1987/Reno, Nevada.

<sup>4</sup>Anderson, John D., Jr., Fundamentals of Aerodynamics, 2nd. Ed., McGraw-Hill, Inc., 1991.